Nuclear matter, nuclear and subnuclear degrees of freedom

Wanda M. Alberico[1,2]

[1] Dipartimento di Fisica Teorica, Università di Torino, via P. Giuria 1, I–10125 Torino, Italy
[2] INFN, Sezione di Torino, Italy

Abstract. We report here theoretical investigations on the complexity of nuclear structure, which have been carried out in the framework of different many–body approaches, typically applied to nuclear matter and quark matter studies. The variational, functional and perturbative scheme are illustrated in their latest developments. The effect of various nucleon–nucleon interactions are tested, particularly in the context of the nuclear response functions, against a large body of experimental data. The properties and decay widths of hypernuclei are shortly revisited, while the equation of state of isospin asymmetric nuclear matter leads us toward nuclear systems of astrophysical interest, like the neutron stars. Finally the transition from hadronic matter to the deconfined phase of quark–gluon plasma endorses the application of many–body and field theoretical techniques to a system with subnucleonic degrees of freedom.

1 Introduction

The subject of this report covers a wide range of items and problems in the theoretical description of nuclear systems, the common link among them being the strong interaction intervening between the constituents of composite systems and the many–body complexity of the latter.

Nuclear and nucleonic structure has been experimentally investigated using probes of quite different nature, whose interaction with the nuclear system involves forces of different nature, from the electroweak one to the most complicated strong interactions between relativistic heavy ions.

We will discuss here at length the information which can be obtained through unpolarized and polarized electron–nucleus scattering, briefly touching also neutrino scattering. Strongly interacting probes, like mesons (π, K) and nucleons will be considered in connection with the specific spin–isospin channels they can excite in a nuclear system.

Finally we will briefly illustrate the problems connected with subnucleonic degrees of freedom, in particular the transition from nuclear matter to quark matter: the so–called deconfinement phase transition, perhaps the only one occurring in the early stages of the Universe which one can hope to reproduce in the laboratory.

Different theoretical schemes are employed to test the performances and limitations of various models for describing nuclear dynamics and spectra. Indeed

in the nuclear medium many degrees of freedom come into play and require different techniques to be enlightened.

For example, sticking to the case of electromagnetic probes, one has to consider not only the one–body nucleonic current, but also the two–body ones, which involve pairs of nucleons correlated via the exchange of charged mesons. In the domain of deep inelastic scattering the high momentum photons exchanged between the electron and the nucleus shed light on the quark structure of the nucleon, namely on the complications associated with the subnucleonic degrees of freedom and colour confinement.

Just mentioning all the above items and themes can give the impression of many different, disconnected fields of research: on the contrary, theoretical and experimental nuclear physics can be viewed as a "magic circle" which involves, with various and strong interrelations, all different subfields. One can start, e.g., from the single nucleon to proceed toward the structure of nuclei and hypernuclei, down to the ideal "nuclear matter" system, then to neutron stars and astrophysical systems, in which realistic models envisage the existence of a quark–gluon plasma phase. And then back, through the confinement mechanism, to nucleons and nuclear systems.

2   Weakly interacting probes: electrons and neutrinos

The main advantage of electron–nucleus scattering stems from the fairly good knowledge of the basic electromagnetic interaction vertex; moreover the virtual exchanged photon can penetrate well inside the nuclear system before being absorbed, thus involving into the process any nuclear constituent in the whole volume of the nucleus. This probe allows to investigate, depending upon the four–momentum transfer, both *nuclear* and *nucleonic* structure. In the second case, which concerns deep inelastic scattering experiments, the partonic structure and perturbative QCD corrections can be tested, together with various quark models for the confined hadronic states.

In the former case, which refers to relatively smaller momentum transfers, nuclear structure studies can be performed by comparing the theoretical evaluation of the inelastic electron scattering cross sections with the measured data, in a wide range of energy and momentum transfers as well as in different experimental setups, appropriate for inclusive (e, e'), one–exclusive $(e, e'p)$, etc. measurements.

In all situations we test the theoretical description of complex nuclei in connection with both the many–body scheme employed and the role played by the NN interaction in shaping cross sections and amplitudes for the excitation of specific nuclear states. Taking advantage from the fact that electrons interact with the whole nuclear volume, one expects that surface effects are of minor importance: thus it is convenient to perform calculations in the framework of nuclear matter.

Both perturbative and variational techniques have been employed to test different model descriptions of:

1. the two (and three)–body nucleon–nucleon interaction
2. the nuclear electromagnetic currents and form factors (including the single nucleon current as well as the two–body, meson exchange currents)
3. the weak nuclear and nucleonic currents (e.g. to investigate the strange form factors of the nucleon)
4. relativistic effects both in the kinematics and in the currents.

All the above items concur in determining the so–called **nuclear response functions**, which can be directly confronted with the ones extracted from the experimental data.

Different types of response functions can be obtained from the cross sections for inelastic electron scattering; we shall list below a few items which have been extensively explored.

$\Diamond$ *Inclusive scattering of unpolarized electrons off nuclei*

In Born approximation the differential cross section (with respect to the energy, ϵ', and the scattering angles, $\Omega \equiv (\theta, \varphi)$, of the final electron) is given by:

$$\frac{d^2\sigma}{d\Omega d\epsilon'} = \sigma_M \left\{ v_L R_L(q, \omega) + v_T R_T(q, \omega) \right\} \tag{2.1}$$

where σ_M is the Mott cross section, $q_\mu^2 = \omega^2 - q^2$ the squared four–momentum transfer, $v_L = (q_\mu^2/q^2)^2$, $v_T = \left[\tan^2(\theta/2) - q_\mu^2/2q^2 \right]$ and $R_{L,T}$ the longitudinal and transverse (separated) electromagnetic nuclear response functions. Relevant physical issues are connected with these response functions, in particular the so–called *Coulomb sum rule* (from the longitudinal response integrated over the energy) and the scaling properties, both in non–relativistic and in relativistic regimes.

$\Diamond$ *Inclusive scattering of polarized electrons (off unpolarized targets)*

From the difference between the **e**–nucleus cross sections, with polarization of the electron parallel and antiparallel to the incident beam it is possible to measure the *asymmetry*:

$$\begin{aligned} \mathcal{A} &= \frac{d^2\sigma^+ - d^2\sigma^-}{d^2\sigma^+ + d^2\sigma^-} \\ &\equiv \mathcal{A}_o \frac{v_L R_{AV}^L(q, \omega) + v_T R_{AV}^T(q, \omega) + v_{T'} R_{VA}^{T'}(q, \omega)}{v_L R_L(q, \omega) + v_T R_T(q, \omega)} \end{aligned} \tag{2.2}$$

which contains, in the numerator, the parity violating (PV) nuclear response functions, stemming from the interference between the nuclear electromagnetic and weak (vector and axial) neutral currents. In the above

$$\mathcal{A}_o = \frac{G_F Q^2}{2\pi\alpha\sqrt{2}} \approx 3.1 \times 10^{-4}\tau \qquad \left(\tau = \frac{Q^2}{4M^2} \right) \tag{2.3}$$

where G_F is the Fermi constant, α the electromagnetic coupling constant, $Q^2 = -q_\mu^2 > 0$ and $v_{T'} = \sqrt{\tan^2(\theta/2) - (q_\mu^2/q^2)} \tan(\theta/2)$. It is worth mentioning that the PV response functions can be sensitive to novel aspects of

the nuclear dynamics, different from the ones explored by the electromagnetic vertex. In particular they give access to the isoscalar NN force and to the neutrons' distribution in nuclei.

◇ *Exclusive versus inclusive electron scattering*

One–exclusive processes, like (e, e', N), in which one nucleon is observed in coincidence with the outgoing electron, are more sensitive tests of the nuclear models. Indeed the probability of a nucleon to be emitted strongly reflects, for example, the momentum distribution inside the nucleus; striking differences are obviously found by employing models like a realistic shell model, the so–called Hybrid model or even the Fermi Gas model (the latter being, manifestly, not appropriate to deal with the details of nuclear structure).

A variety of nuclear response functions can be separated by an adequate selection of the kinematics; in particular some interference between the longitudinal and transverse components of the electromagnetic current contribute to the one–exclusive cross sections, at variance with the inclusive ones. Thus one can test different components and matrix elements of the nuclear electromagnetic current, including delicate questions like the off–shellness of the nucleonic current in the nucleus, the contribution of meson exchange currents, the limitations of non–relativistic approaches.[1, 2]

Finally (e, e', N) is fairly sensitive to the strong interaction of the ejected nucleon with the residual nucleus, the so–called final state interaction (FSI), which can be responsible for a sizeable distortion of the outgoing nucleon wave. Recently a semiclassical approach has been proposed[3] to describe this specific aspect: it will be shortly mentioned here, since it provides a natural bridge between nuclear matter and finite nuclei. The main research activity on the electromagnetic interaction in light nuclei is reported elsewhere[4].

Coming back to the main subject of this report, we shall now concentrate on the different theoretical methods which have been employed for an accurate evaluation of the electromagnetic response functions in nuclear matter. They can be roughly grouped into three categories:

1. The variational method, which is based on the Fermi Hypernetted Chain (FHNC) scheme
2. The functional method, which employs the path–integral approach for developing a consistent bosonic loop expansion
3. The traditional perturbation theory, which encompasses the most frequently utilized models, from the Fermi gas (non–relativistic and relativistic), to the Hartree–Fock (HF) model combined together with the important correlations provided by the Random Phase Approximation (RPA).

In concluding this section we briefly mention the case of neutral current (NC) neutrino– and antineutrino–nucleus scattering: these processes offer the possibility to extract information on the strange form factors of the nucleon. For

this purpose two quantities have been considered, the $\nu - \bar{\nu}$ asymmetry[5]:

$$\mathcal{A}_p = \frac{(\sigma)^{NC}_{\nu p \to \nu p} - (\sigma)^{NC}_{\bar{\nu} p \to \bar{\nu} p}}{(\sigma)^{CC}_{\nu n \to \mu^- p} - (\sigma)^{CC}_{\bar{\nu} p \to \mu^+ n}} \tag{2.4}$$

and the ratio of the cross sections for inelastic NC scattering of $\nu(\bar{\nu})$ on nuclei, with the emission of a proton or, respectively, of a neutron:

$$\mathcal{R}^{\nu(\bar{\nu})}_{p/n} = \frac{(\sigma)^{NC}_{\nu(\bar{\nu}),p}}{(\sigma)^{NC}_{\nu(\bar{\nu}),n}} . \tag{2.5}$$

Calculations of both (2.4) and (2.5) have been performed, in an energy range from 200 MeV to 1 GeV, within two relativistic independent particle models (Fermi gas and shell model); the final state interactions of the ejected nucleon have been taken into account through relativistic Optical model potentials.[6, 7, 8].

While the values of the cross sections significantly depend on the nuclear model (especially in the lower energy range), the NC/CC neutrino–antineutrino asymmetry and the ratio p/n show a rather mild dependence on the model and allow one to disentangle different values of the strangeness parameters entering into the weak NC axial and vector strange form factors of the nucleon.

We remind that the $Q^2 = 0$ limit of the axial strange form factor, g^s_A, is closely related to the problem of the proton spin, a long lasting puzzle raised by the measurements, in the deep inelastic polarized lepton scattering, of the polarized structure function g_1 of the proton. Moreover the information on the strange form factors of the nucleon extracted fron neutrino scattering is complementary to the similar information, which can be obtained in the above quoted PV polarized electron scattering experiments.

3   Electromagnetic response functions

3.1   Variational method

The inclusive *transverse response function* of symmetric nuclear matter at saturation density, $R_T(q, \omega)$, has been studied by Fabrocini[9] within the Correlated Basis Function (CBF) perturbation theory. The main goal of this work is to ascertain how R_T is affected by the NN correlations, with a special emphasis on the MEC contributions.

CBF calculations are based upon a set of correlated wave functions

$$|n> = \mathcal{S} \left[\prod_{i,j} f(i,j) \right] |n>_{FG} \tag{3.6}$$

obtained by applying a symmetrized product of two–body correlation operators, $f(i, j)$, to the FG states $|n>_{FG}$. The following effective structure is adopted for f:

$$f(i, j) = \sum_{q=1,6} f^{(q)}(r_{ij}) O_{ij}^{(q)}, \qquad (3.7)$$

$$O_{ij}^{(q=1,6)} = (1, \sigma_i \cdot \sigma_j, S_{ij}) \otimes (1, \tau_i \cdot \tau_j) \qquad (3.8)$$

S_{ij} being the tensor operator; $f(i, j)$ depends upon a set of variational parameters, which are fixed by minimizing the expectation value of a realistic, non–relativistic Hamiltonian on the correlated ground state. The g.s. energy is calculated via the FHNC cluster summation technique, using the correlation corresponding to the Argonne V_{14} + Urbana VII three–nucleon interaction model of ref.[10].

The Jastrow (scalar) component of (3.8) accounts for the short range NN repulsion, while, among the remaining correlators, the most relevant are the spin–isospin and the tensor–isospin ones, which mostly stem from the one–pion exchange (OPE) long range part of the potential.

Configurations up to correlated one particle–one hole (1p–1h) intermediate states are considered; the spreading due to the decay of particle (hole) states into 2p–1h (2h–1p) states is taken into account via a realistic optical potential model.

The transverse response is given by

$$R_T(q, \omega) = \frac{1}{A} \sum_n |< 0|\mathbf{j}(\mathbf{q})|n >|^2 \delta(\omega - \omega_n) \qquad (3.9)$$

where the sum goes over the intermediate excited states $|n>$, with excitation energy ω_n; $\mathbf{j}(\mathbf{q})$ is the electromagnetic current operator

$$\mathbf{j}(\mathbf{q}) = \mathbf{j}^{(1)}(\mathbf{q}) + \mathbf{j}^{(2)}(\mathbf{q}) \qquad (3.10)$$

sum of the one–body, magnetic current $[\mathbf{j}^{(1)}(\mathbf{q})]$ and the two–body exchange currents $[\mathbf{j}^{(2)}(\mathbf{q})]$. For the latter, the Schiavilla–Pandharipande–Riska model[11] is adopted, which satisfies, by construction, the continuity equation with realistic V_{14} Argonne and Urbana potentials. Currents due to intermediate Δ–isobar excitations are also included. The sharp energy boundaries of the 1p–1h FG response are smoothed out by an appropriate folding with a width $W(\omega)$:

$$R_T(q, \omega) = \frac{1}{\pi} \int d\omega' R_T^{1p-1h}(q, \omega') \frac{W(\omega')}{(\omega - \omega')^2 + [W(\omega')]^2}, \qquad (3.11)$$

where $W(\omega) = \text{Im} W_o(\omega)/M^*$, W_o being the optical potential and M^* the nucleon effective mass.

Fig. 1 shows the comparison of the nuclear matter response evaluated in ref.[9] and the experimental data on ^{40}Ca; both the impulse approximation (IA) and the full calculation (MEC+IA) are shown. The data are taken from from
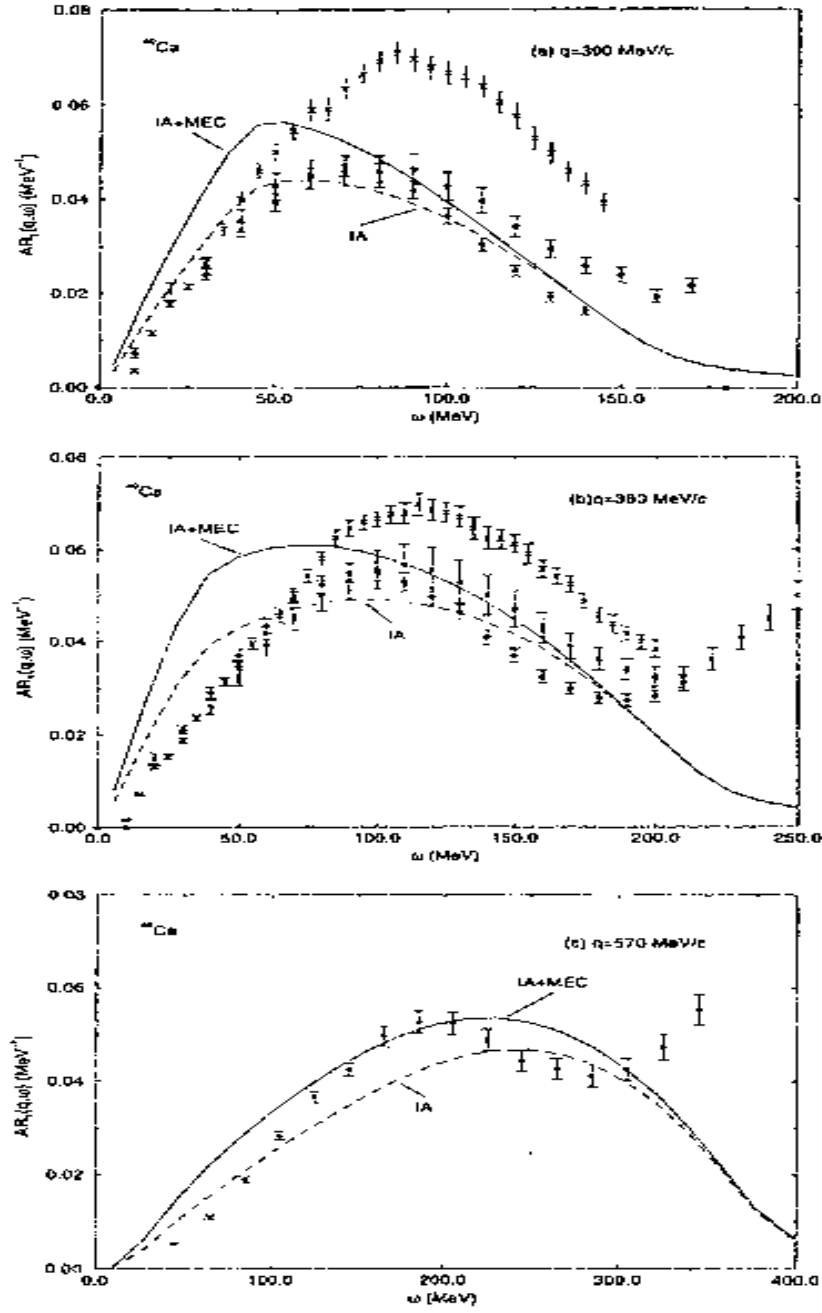
Fig. 1. Transverse response at $q = 300$ (a), 380 (b), and 570 (c) MeV/c for ^{40}Ca and nuclear matter. See text.

ref.[12] ($\times$), ref.[13] (circles) and ref.[14] (black circles). The global contribution of the two–body currents turns out to be positive and provides an enhancement of the one–body response, ranging from $\sim 20\%$ for the lower momenta (300 MeV/c) to $\sim 10\%$ for the higher ones (about 500 MeV/c). The tensor–isospin component of the correlation is crucial to obtain these results.

Several variational calculations have been performed in the past for the *longitudinal response function* as well, both in nuclear matter and light nuclei. In a recent work Amaro *et al.*[15] have tested a simple approximation to deal with the short range correlations (SRC) affecting the 1p–1h excited states, which build up the nuclear response functions.

The basic idea of the model (previously tested for the ground state properties) consists in truncating the CBF expansion in such a way to retain only those terms containing a single Jastrow–type correlation line,

$$h(r) = f^2(r) - 1 \,. \tag{3.12}$$

The expansion in powers of $h(r)$ has the property of conserving the proper normalization of the correlated many–body wave function. The nuclear charge is conserved as well, at variance with other truncation schemes. The correlation employed is the scalar component of a complicated state dependent correlation, fixed to minimize the nuclear binding energy in a FHNC calculation with the Urbana V_{14} NN potential.

Fig. 2 shows the diagrams retained in [15]. The comparison between the calculation of the longitudinal response function in the full FHNC and in the proposed approximation shows that the difference between the corresponding results does not exceed a few parts $\times 10^{-4}$, in a fairly large interval of momentum transfers. This proves the reliability of the truncated scheme also for dealing with 1p–1h excited states; it needs to be further tested, however, for the 2p–2h responses.

3.2   Functional (path integral) method

The path integral approach offers a consistent theoretical foundation of the nuclear response functions. Indeed it employs the approximation schemes of QFT, namely the perturbative approach and the loop expansion, to provide a fully consistent criterium of selecting classes of diagrams, still preserving the fundamental symmetries and invariances of the choosen model Lagrangian.

Starting from a Lagrangian which describes interacting nucleons, pions and eventually ρ mesons, all coupled to an external electromagnetic field, one derives the nuclear polarization propagator and response functions through derivatives of the generating functional

$$\begin{aligned}
Z[j_\mu^{ext}] &= \frac{1}{\mathcal{N}} \int \mathcal{D}\left[\bar{\psi}, \psi, \Phi, A_\mu\right] \exp\left\{i \int dx [j_\mu^{ext} A_\mu]\right\} \\
&\times \exp\left\{i \int dx \left(\mathcal{L} + \mathcal{L}_{em} + J_\mu A^\mu + B_{\mu\nu} A^\mu A^\nu\right)\right\}
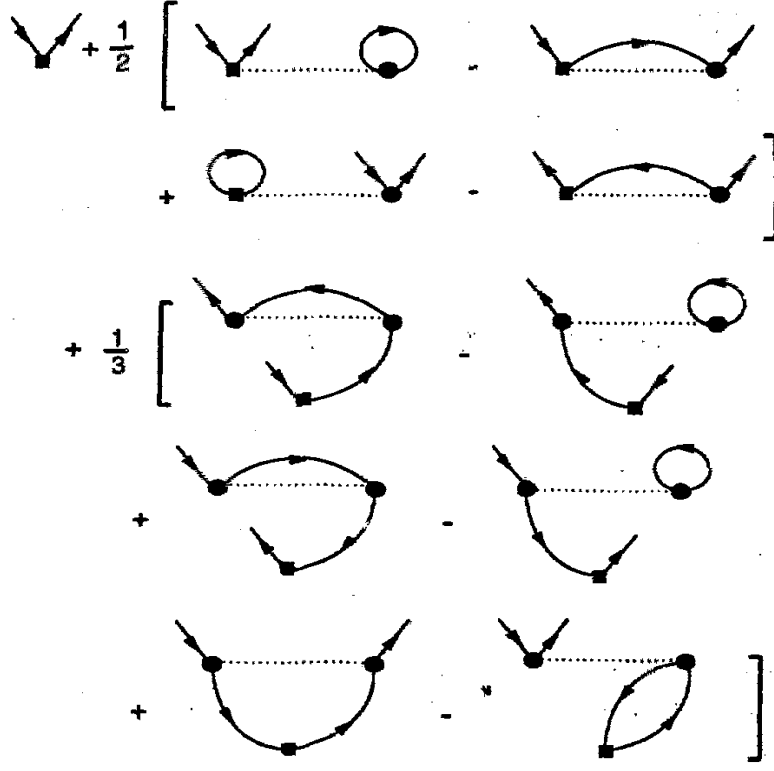\end{aligned} \tag{3.13}$$

Fig. 2. Diagrams considered in the model of ref.[15]. The dotted lines represent the correlation function. The oriented lines represent particle and hole wave functions. The black circle indicates an integration point, while the black squares indicates the integration point, where the charge operator is acting.

where $\psi, \bar{\psi}$ are the nucleon fields, Φ and A_μ, respectively, the pion and electromagnetic fields and $\jmath_\mu^{ext}$ the external source of the latter. In the above

$$\mathcal{L} = \bar{\psi}(i\gamma^\mu\partial_\mu - M)\psi + \tfrac{1}{2}(\partial_\mu\Phi)^2 - \frac{m_\pi^2}{2}\Phi^2 - ig\bar{\psi}\gamma_5\tau\psi \cdot \Phi \qquad (3.14)$$

is the model Lagrangian (without the ρ meson) and

$$J_\mu = e\bar{\psi}\tfrac{1}{2}(1+\tau_3)\gamma_\mu\psi + e[\Phi \times \partial_\mu\Phi]_3 \qquad (3.15)$$

$$B_{\mu\nu} = e^2 g_{\mu\nu}\Phi^+\Phi^- \qquad (3.16)$$

the required couplings of nucleons and pions to the e.m. field. The results obtained, within this formalism, for the longitudinal and transverse responses in the inclusive electron scattering are shown in the work by Cenni *et al.*[16]

It is worth mentioning that an important connection between the variational technique and the path integral approach has been recently explored in ref.[17]. These authors suggest a new method, based on the variation, within a path integral framework, of a trial Hamiltonian: it turns out that a particular choice of the latter corresponds exactly to the use of a Jastrow correlated Ansatz for the wave function in the FHNC approach. Thus the new formalism generalizes the FHNC and CBF techniques, allowing for their extension to relativistic and field theoretical problems.

3.3   Perturbation theory

Several approaches based on perturbative schemes have been applied to the evaluation of nuclear response functions both for inclusive (parity conserving and parity violating) and exclusive processes. Most calculations are based on non–relativistic Hamiltonians and currents, but attempts to include relativistic effects, especially in the electromagnetic currents and vertices, have been done.

Many–body perturbative techniques have been developed to treat quasielastic electron scattering in nuclear matter. The Green's function method is particularly suited to express inelastic cross sections through the imaginary part of the polarization (particle–hole) propagator; nuclear matter results compare fairly well with the experimental data for energy transfers in the region of the quasielastic peak and above, providing the Δ_{33} resonance and mesonic degrees of freedom are incorporated in the nuclear matter polarization propagators.

The role played by the NN interaction in reshaping the nuclear matter response functions with respect to the pure FG one has been widely investigated, by employing both phenomenological effective interactions and G–matrix parameterizations based on the one–boson exchange potential. Starting from the naive Fermi gas description, one can easily obtain the Hartree–Fock (HF) or Brueckner–Hartree-Fock (BHF) polarization propagators; the next step is then to include RPA correlations, both in the "minimal" version of the so–called *ring* diagrams and in the framework of the fully antisymmetrized RPA.

Numerical calculations of the HF+RPA response functions can require large computing time. Indeed, although in nuclear matter the ring approximation for the polarization propagator can be analytically evaluated, as soon as one dresses the particle and hole propagators with HF self–energies, even the simple HF p–h propagator, $\Pi_{HF}(q, \omega)$, requires numerical integrations when the HF self–energy is derived from any realistic NN interaction.

Moreover the simple algebraic equation for the ring polarization propagator turns into an infinite series of complex integrals when the exchange matrix elements of the p–h interaction are taken into account in the fully antisymmetrized RPA, which is diagrammatically shown in Fig. 3. An approximate, but reliable, treatment of these contributions is thus compulsory.

This has been achieved with the method of the *continued fraction* (CF) expansion[18], which will be briefly sketched in the following. The CF–like ex-
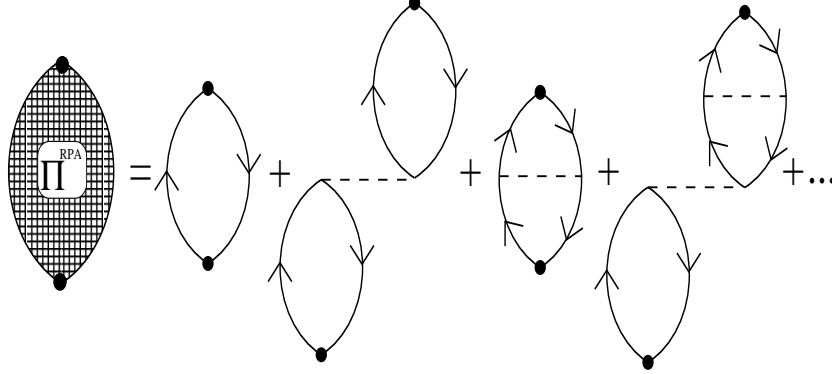
Fig. 3. Diagrammatic representation of the perturbative expansion for the polarization propagator in RPA. The dashed line represents the particle–hole interaction V.

pansion for the polarization propagator can be written as

$$\Pi^{RPA} = \cfrac{\Pi^{(0)}}{1 - A - \cfrac{B}{1 - C - \cfrac{D}{1 - \ldots}}} \tag{3.17}$$

where $\Pi^{(0)}$ is the free (or HF) particle–hole propagator and all symbols appearing in (3.17) are functions of both the energy and momentum transfers. The CF approach at n–th order reproduces exactly the perturbative series expressing the antisymmetrized RPA at the same order while it approximates higher orders. Setting, for example,

$$\Pi^{RPA} = \sum_{n=0}^{\infty} \Pi^{(n)} \tag{3.18}$$

the first order in CF provides the following approximation for $\Pi^{(n)}$:

$$\Pi^{(n)} \simeq \Pi^{(0)} \left[\frac{\Pi^{(1)}}{\Pi^{(0)}} \right]^n , \tag{3.19}$$

where $\Pi^{(1)} \equiv \Pi^{(0)} 4V \Pi^{(0)} + \Pi^{(1)ex}$ is the sum of the direct and exchange first order terms. With this approximation the summation in (3.18) is trivial, yielding

$$\Pi_{CF1}^{RPA} = \frac{\Pi^{(0)}}{1 - \Pi^{(1)}/\Pi^{(0)}} = \frac{\Pi^{(0)}}{1 - 4V\Pi^{(0)} - \Pi^{(1)ex}/\Pi^{(0)}} . \tag{3.20}$$

The next step extends the approximation to the exact second order term; the corresponding RPA propagator reads:

$$\Pi_{CF2}^{RPA} = \frac{\Pi^{(0)}}{1 - \Pi^{(1)}/\Pi^{(0)} - \left\{ \Pi^{(2)}/\Pi^{(0)} - [\Pi^{(1)}/\Pi^{(0)}]^2 \right\}} \tag{3.21}$$

$$= \frac{\Pi^{(0)}}{1 - 4V\Pi^{(0)} - \Pi^{(1)ex}/\Pi^{(0)} - \left\{\Pi^{(2)ex}/\Pi^{(0)} - [\Pi^{(1)ex}/\Pi^{(0)}]^2\right\}} \, ,$$

where the approximation provided by the first order CF expansion has been subtracted off.

Numerical calculations for the longitudinal and transverse responses, using a G–matrix based on the Bonn potential, show that the CF expansion rapidly converges, giving a few percent correction between the first and the second order CF results. On the contrary, the differences between ring and RPA (in the CF1 or CF2 approximation) responses appear to be sizeable, both in the longitudinal and in the transverse channel, with, perhaps, the exception of the spin–isovector channel, as it is illustrated in Fig. 3. We also remind here that a very useful (and accurate) approximation, consisting in a "bi–parabolic" parameterization of the HF self–energy of the nucleon[19], allows to express analytically Π_{HF}, thus considerably reducing the computational time.

Within the perturbative approach it is also possible to deal with *relativistic effects*, which might become important for energy/momentum transfers larger than 0.5 GeV or so. Besides the corrections stemming from the relativistic kinematics and vertices, which have been completely taken into account in the framework of the Fermi gas model, several investigations, based on a fully relativistic Lagrangian with nucleonic and pionic degrees of freedom, both coupled to the external electromagnetic field, have been performed. These approaches usually include both the single–nucleon e.m. current and the two–body MEC and account for relativistic effects within an expansion in terms of suitably "small" variables, like the energy/momentum transfers in units of twice the nucleon mass ($\kappa = q/2M, \lambda = \omega/2M$). A new relativistic expansion for the matrix elements of one– and two–body e.m. currents has been recently proposed by Amaro *et al.*[1] in terms of the parameters $\eta_i \equiv p_i/M$ (characteristically of the order of $1/4$), $\{p_i\}$ being the initial–state nucleon momentum inside the nucleus: clearly this formalism will be especially suited in the regime of GeV energies, where, on the contrary, κ and λ are no longer small with respect to 1.

y–scaling and Coulomb sum rule The concepts of y–scaling and Coulomb sum rule have been throughly discussed in the past since they offer important tests for the accuracy and reliability of the nuclear model description underlying the calculation of the electromagnetic response functions. Both of them require a careful investigation in order to disentangle, from the full expression of the longitudinal and transverse response functions, those dividing factors such that the reduced responses have scaling properties or (for what concerns the longitudinal response) satisfy the Coulomb sum rule. This task is not trivial since, as shown by the Relativistic Fermi Gas (RFG) model, the e.m. form factors to be divided by are not simply factorizable, due to the structure of the relativistic one–nucleon current.

In the work by Barbaro *et al.*[20] the dividing factors G_L, G_T are constructed in the RFG for the longitudinal and transverse response functions in such a way
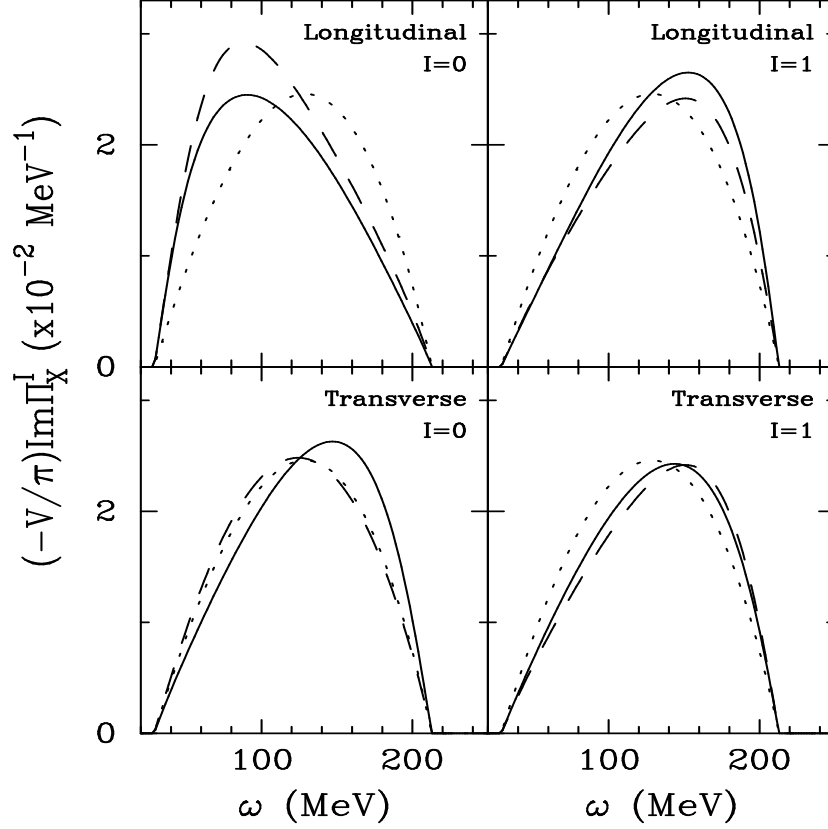
Fig. 4. Nuclear matter responses for $k_F = 195$ MeV/c at $q = 500$ MeV/c: the dotted line corresponds to the free response, the dashed one to the ring approximation and the solid line to the RPA–CF1 response. The kinematics is relativistic and the particle–hole interaction is derived from a realistic G–matrix.

that the reduced responses, so obtained, scale; another dividing factor, H_L, yields a (different) reduced response which fulfills the Coulomb sum rule (CSR). The relevant point here is that G_L, G_T and H_L are all found to be only weakly model–dependent, thus providing essentially universal dividing factors. It becomes thus possible to test whether specific models scale and satisfy the CSR. This investigation has been carried out for the Hybrid model[2] and the Quantum Hadrodynamic model[21] (QHM), each one with different types of interaction effects which go beyond the strict RFG. It is found that while the Hybrid model scales and obeys the CSR, the QHM does neither. The Coulomb and higher order sum rules have also been investigated by Amore *et al.*[22] in the RFG, by employing two different methods, namely by exploiting the scaling properties of the longitudinal response function and by enforcing the completeness of the

states in the space–like domain via the Foldy–Wouthuysen transformation.

3.4   Exclusive versus inclusive electron scattering scattering

The connections between exclusive and inclusive electron–nucleus scattering within the framework of the plane–wave impulse approximation (PWIA) have been investigated in a work by Cenni *et al.*[2]. These authors test the interplay between the (model independent) kinematical constraint and the (model dependent) features of the spectral function in providing the exclusive (and inclusive) nuclear responses. The RFG and the Hybrid model are employed to provide a link between finite and infinite Fermi systems and to assess the impact of the confinement of the struck nucleons on the inclusive charge response. One of the important outcomes of this work is that, with an energy–shift and rescaled Fermi momentum, an effective RFG response can be obtained whose first three energy–weighted moments agree quite well with the analogous quantities evaluated within the (confined) Hybrid model.

A more recent work[3] evaluates semi–classically the exclusive (e, e', p) cross sections, yet partially preserving the simplicity of nuclear matter calculation, but going beyond the PWIA. Indeed this approach allows to include the distortion of the outgoing nucleon wave (the so–called final state interaction, FSI) at least within the mean field approximation.
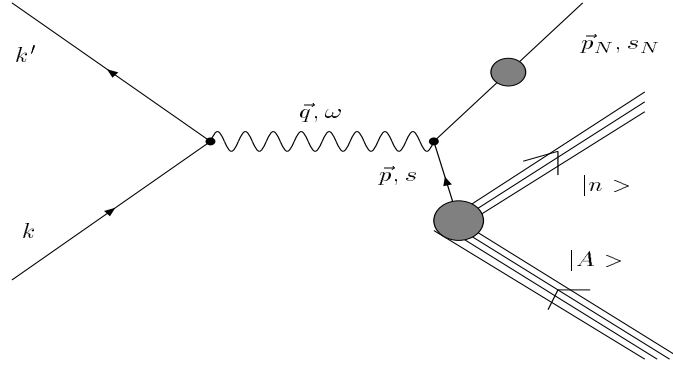

Fig. 5.

Sticking to the IA, the cross section for the (e, e', p) scattering process, which is schematically illustrated in Fig. 5, reads:

$$\frac{d^4\sigma}{d\epsilon' d\Omega_e dE_N d\Omega_N} = E_N p_N \left(\frac{d\sigma}{d\Omega_e}\right)_{eN} S(\mathbf{p}_m, \mathcal{E}). \qquad (3.22)$$

In the above:

$$\left(\frac{d\sigma}{d\Omega_e}\right)_{eN} = \sigma_{Mott}\frac{1}{\cos^2(\theta/2)}\frac{m_e^2}{\epsilon\epsilon'}\eta^{\mu\nu}\frac{M^2}{E(\mathbf{p})E_N}W_{\mu\nu}(\mathbf{p},\mathbf{p}+\mathbf{q}) \qquad (3.23)$$

is the single nucleon cross section, while

$$S(\mathbf{q},q_0) = \frac{1}{(2\pi)^3}\frac{M}{E(\mathbf{q})}\frac{< A|\hat{a}_q^{\dagger}\delta\left(q_0 - \hat{\mathcal{H}} - \mu\right)\hat{a}_q|A >}{< A|A >} \qquad (3.24)$$

is the nuclear spectral function, which in (3.22) depends upon the missing momentum $\mathbf{p}_m = \mathbf{q} - \mathbf{p}_N$ and the missing energy $\mathcal{E} = E_N - \omega$ (see Fig. 5 for the other symbols).

Different nuclear models generally provide different spectral functions, as one can see, for example, by comparing the ones obtained in the RFG,

$$S^{RFG}(\mathbf{p},\mathcal{E}) = \frac{\Omega}{(2\pi)^3}\theta(k_F - p)\delta\left\{\mathcal{E} - \sqrt{k_F^2 + M^2} - \sqrt{p^2 + M^2}\right\} \qquad (3.25)$$

and in the Hybrid model (harmonic oscillator bound states combined with a continuum of unbound states):

$$S^{HM}(\mathbf{p},\mathcal{E}) = \sum_{N=0}^{N_{max}}\delta\left\{\mathcal{E} - (N_{max} - N)\omega_0\right\}n_N(p), \qquad (3.26)$$

where

$$n_N(p) = \sum_{n,\ell=N-2n}\frac{2\ell + 1}{4\pi}|\varphi_{n\ell}(p)|^2 \qquad (3.27)$$

is the momentum distribution for the N–th shell. The spectral function (3.26) is illustrated in Fig. 6, where a dashed line is drawn in correspondence with the support for the spectral function of the RFG, eq. (3.25), which is infinite along that line and zero elsewhere.

Within the semiclassical framework, the Wigner transform of the spectral function reads:

$$[S(\mathcal{E})]_W(R,\mathbf{p}) = \theta\left[\epsilon_F - \frac{p^2}{2M^*} - V(R)\right]\delta\left\{\mathcal{E} - \left[\epsilon_F - \frac{p^2}{2M^*} - V(R)\right]\right\} \quad (3.28)$$

where $V(R)$ is a suitable shell model potential (e.g. the harmonic oscillator or the Woods–Saxon potentials) and $\epsilon_F \equiv k_F^2(R)/2M^* + V(R)$ the local Fermi energy. It is shown in ref.[3] that in the semiclassical approach it is possible to account for the distortion of the ejected nucleon (illustrated by the black dot in Fig.5) in a relatively simple way: an appropriate distortion operator is introduced, for which two heuristic assumptions are made, corresponding to the eikonal and to the uniform approximations, respectively. The corresponding exclusive cross sections turn out to be quite different, hence stressing the relevance of the FSI in the analysis of the exclusive processes.
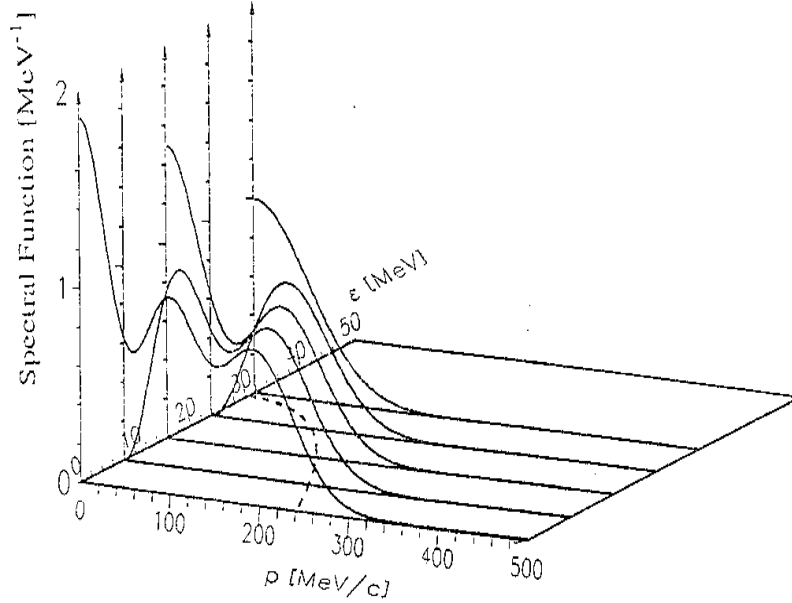
Fig. 6. The spectral function in the Hybrid Model.

4 Strange probes and strange matter

4.1 K^+–nucleus scattering

The quasielastic K^+–nucleus scattering has been thoroughly investigated by De Pace *et al.*[23, 24, 25]. This subject shares several motivations with the items in the previous sections. The first one relies on the relatively small (as compared with strong interaction processes) K^+N cross sections: as a consequence the K^+ projectiles can penetrate deeply inside the nucleus, similarly to electrons and photons, thus allowing to investigate collective effects in the nuclear response. The second reason of interest is the possibility of exploring scalar–isoscalar excited states, which are the dominant channel for the K^+–nucleon coupling. This channel can be partly explored in the longitudinal electron scattering response functions, but an isospin separation in addition to the customary longitudinal–transverse one has never been, till now, carried out in (e, e', X) experiments.[1] Finally the observed excess in elastic K^+–nucleus scattering cross sections seems

---

[1] Such a separation should become possible with PV electron scattering experiments and it will be of extreme interest to compare the latter with the K^+ quasielastic scattering.

to require, to be explained, some enhancement induced by the nuclear medium itself.

A simple phenomenological approach, which expresses the above mentioned cross sections by means of an effective number of participant (N_{eff}),

$$\frac{d^2\sigma}{d\Omega d\omega} = N_{eff} \frac{d\sigma_{K^+N}}{d\Omega} R(q,\omega), \qquad (4.29)$$

seems to require values of N_{eff} too large with respect to what expected in the Glauber theory; moreover (4.29) fails in describing the observed collective phenomena at low momentum transfer.

The model proposed in [23] allows to evaluate the nuclear response $R(q,\omega)$ within a continuum RPA, using an effective G–matrix particle–hole interaction and a Woods Saxon mean field, complemented by an appropriate spreading width of the ph states. The kinematics is relativistic. An improved Glauber theory is used for the reaction mechanism, including one– and two–step contributions.
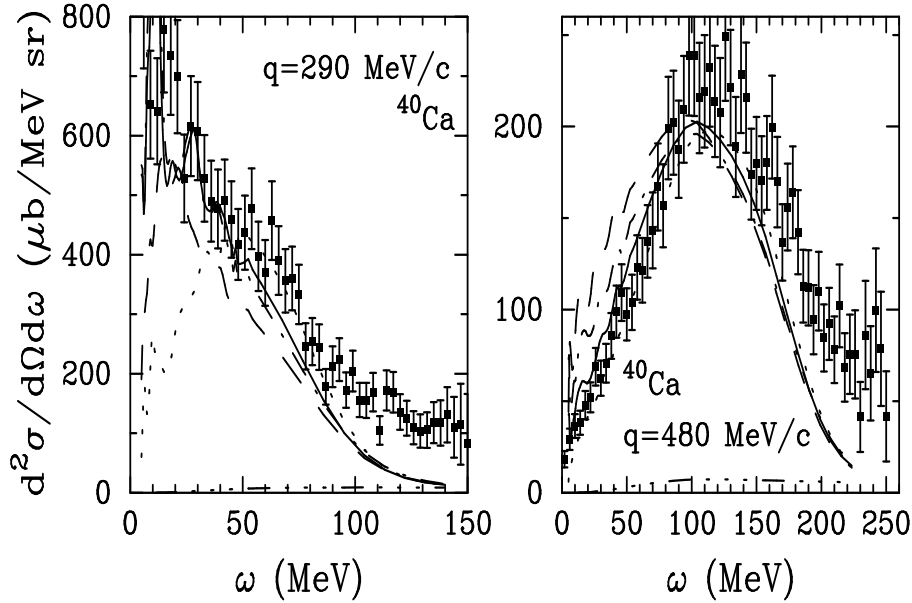

Fig. 7. The K^+-^{40}Ca cross sections at $q = 290$ MeV/c (left) and $q = 480$ MeV/c (right); data are taken from ref.[26]. For the explanation of the theoretical curves see text.

In Fig. 7 we show an example of the results obtained in this framework: the experimental data for K^+-^{40}Ca scattering are compared with the 1 step (free)+ 2 step calculation (dotted line), the 1 step (using the N_{eff} formula)+ 2 step (dot-dashed line) and the 1 step (RPA)+ 2 step (dashed line). While the free

response is clearly inadequate to reproduce the data, the other two calculations fail in reproducing the excess cross section appearing in the low energy region at small momentum transfers. However if one empirically reduces by about 50% the effective ph interaction in the scalar isoscalar channel, then the 1 step (RPA)+ 2 step turns out to be in very good agreement with the experimental data, in the whole range of momentum transfers and nuclei (^{12}C and ^{40}Ca) explored. This is a new, challenging information on the ph force acting in this channel.

4.2   Hypernuclei (structure and decay)

In the previous paragraph we have considered the interaction of a strange particle, the $K^+(\bar{s}u)$, with the nuclear medium. Should a $K^-(s\bar{u})$ hit a nucleus, most of the times it gets absorbed by a nucleon, leading to the formation of a hypernucleus, namely a nucleus containing one (or more) hyperon (sqq). The lightest and more easily produced hyperon is the Λ particle and a great interest is focussed on the investigation of the ground state properties and decay mechanisms of Λ–hypernuclei. Several experimental data are already available on light and medium hypernuclei, but a reacher set of measurements are expected from the FINUDA experiment, which is just starting operating in the Frascati National Laboratory of INFN.

The **weak decay width** of Λ–hypernuclei can be evaluated with the Green's function (polarization propagator) method, which is conveniently implemented in nuclear matter and extended to finite systems through the so–called Local Density Approximation (LDA). The width of the hypernucleus is derived from the Λ self–energy

$$\Gamma_\Lambda(k,\rho) = -2\mathrm{Im}\Sigma_\Lambda(k,\rho) \qquad (4.30)$$

after integrating over the Λ momentum distribution.

Three different mechanisms contribute to the weak decay of a Λ in the nucleus:

- the *mesonic decay*,

$$\Lambda \longrightarrow \pi N \qquad (\Gamma_M),$$

  which also occurs in free space and is relevant only in light hypernuclei, since the Pauli blocking prevents the low–momentum outgoing nucleon to be emitted in a medium–heavy nucleus;
- the *two–body non–mesonic (NM) decay*

$$\Lambda N \longrightarrow NN \qquad (\Gamma_1),$$

- the *three–body non–mesonic decay*

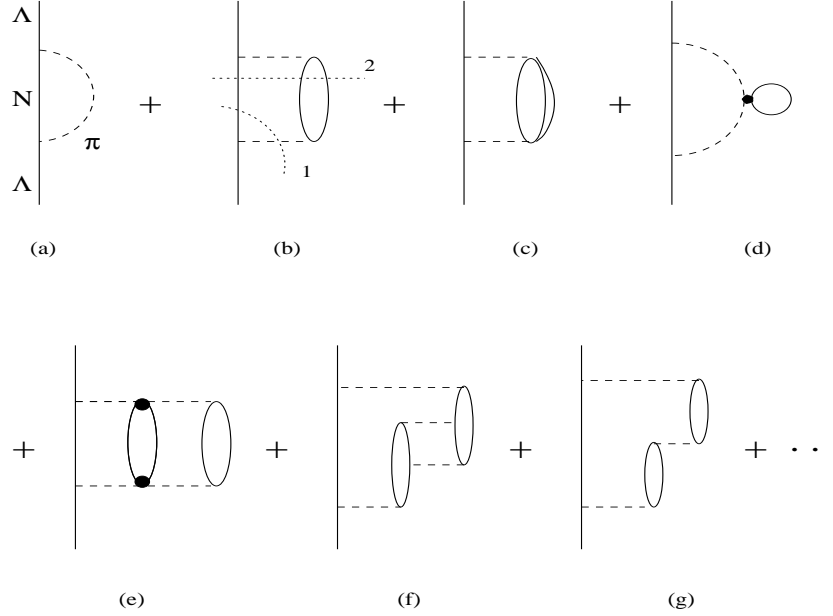$$\Lambda NN \longrightarrow NNN \qquad (\Gamma_2).$$

Fig. 8. Lowest order terms for the Λ self–energy in nuclear matter.

A new evaluation of the Λ self–energy has been carried out[27], which includes the 1p-1h and 2p-2h polarization propagators (related to Γ_1 and Γ_2, respectively) in a RPA scheme. Fig. 8 illustrates a few examples of the diagrams whose imaginary part is contributing to the hypernuclear decay width. The particle–hole interaction embodies the exchange of π and ρ mesons, together with short range repulsive correlations described by the two Landau–Migdal parameters, g' and g'_Λ (the latter being used when one vertex of the exchanged pion coincides with the weak $\Lambda\pi N$ vertex). The nuclear matter calculation is adapted to finite nuclei using the LDA, which amounts to replace the constant Fermi momentum with a local one, expressed by $k_F(r) = [3\pi^2\rho(r)/2]^{1/3}$, $\rho(r)$ being the nuclear density. The width associated to the decay of a Λ with momentum k is then

$$\Gamma_\Lambda(\mathbf{k}) = \int d\mathbf{r}|\psi_\Lambda(\mathbf{r})|^2\Gamma_\Lambda[\mathbf{k},\rho(r)] \tag{4.31}$$

where $\psi_\Lambda(\mathbf{r})$ is the Λ wave function in the nucleus. The results one obtains turn out to be very sensitive to the latter, the best choice corresponding to a Woods Saxon potential well which reproduces the measured s and p energy levels of the Λ in the nucleus. Finally the total width of the hypernucleus is obtained by integrating (4.31) over the momentum distribution of the Λ itself:

$$\Gamma_\Lambda = \int d\mathbf{k}\,|A_\Lambda(\mathbf{k})|^2\,\Gamma_\Lambda(\mathbf{k}). \tag{4.32}$$

The results obtained within this framework are illustrated in Fig. 9, where the decay width of several hypernuclei (from the "light" ^{12}C to the heaviest ^{209}Bi and ^{238}U) is shown, in units of the free Λ decay width, Γ_{free}, as a function of the mass number. The separate contributions, Γ_M, Γ_1 and Γ_2, are also displayed.

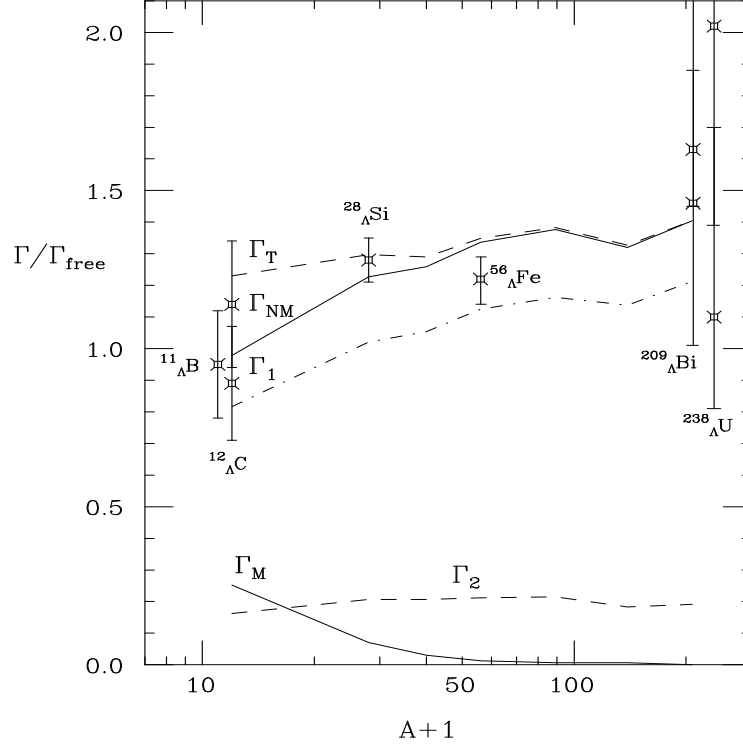**Fig. 9.** Λ decay widths in finite nuclei as a function of the mass number A; the labels of the various curves correspond to: the mesonic width (Γ_M), the one– (Γ_1) and two–body (Γ_2) induced decay widths, the total non–mesonic width ($\Gamma_{NM} = \Gamma_1 + \Gamma_2$) and the total ($\Gamma_T$), sum of all independent contributions.

The theoretical results are in good agreement with the data over the whole hypernuclear mass range explored. The saturation property of the $\Lambda N \rightarrow NN$ interaction in nuclei clearly appears in the flattening of the decay width as the mass number increases. In spite of these satisfactory results, there remains to be explained the large experimental value of the ratio Γ_n/Γ_p, which does not seem to be in agreement with the present theoretical schemes.

Concerning the **ground state properties of hypernuclei** we should mention here a research project by Co *et al*[28], who intend to investigate the structure of hypernuclei within the FHNC scheme. Starting from a suitable basis of

single particle wave functions (Woods–Saxon and/or HF wave functions with finite range interaction) a Jastrow correlated many–body state will be obtained by developing a FHNC formalism for a system of A nucleons plus one impurity (the hyperon). Binding energy and first excited states can also be calculated.

5   Asymmetric nuclear matter

5.1   Equation of state of asymmetric matter

Nuclear matter is usually considered as an isospin symmetric system, $Z = N = A/2$, where the Coulomb interaction between protons is switched off. In reality heavier nuclei are more and more isospin asymmetric, the larger number of neutrons being there to balance the increasing Coulomb repulsion. An interesting, ideal extension of these systems is the asymmetric nuclear matter, where the neutron excess is measured by the asymmetry parameter $I = (N - Z)/A$.

Several investigations have been performed on the ground state properties of (strongly) asymmetric nuclear matter, with large asymmetry parameter, up to values as large as 0.8. In the extreme limit $I \to 1$ one obtains neutron matter, which is obviously unbound as far as nuclear forces are concerned, but deserves very interesting applications in the description of neutron stars, which are bound by gravitational force, but can be considered as a unique realization of this ideal system.

The equation of state of asymmetric nuclear matter contains a symmetry term which depends upon the asymmetry parameter and the density of the system; the equilibrium conditions are crucially determined by the NN interaction: various effective forces can produce quite different behaviours with ρ in the potential energy contribution to the symmetry energy.[29]

A study of non–equilibrium properties of asymmetric nuclear matter has been carried out by Di Toro *et al.*[30] starting from two Vlasov equations, for proton and neutron liquids, coupled through the mean field. The unstable growth of density perturbations is influenced by the initial asymmetry: in neutron rich nuclear matter the formation of larger fragments, in which isospin symmetry is restored, is favoured.

At low (subsaturation) densities the system develops collective dynamical instabilities of isovector nature, the so–called *spinodal decomposition*: it corresponds to the growth of density pertubations leading to a liquid–gas phase separation in which symmetric nuclei coexist with a neutron gas. The instability region (for example in the (T, ρ) plane, turns out to be reduced in strongly asymmetric systems.

This phenomenon can be tested in heavy ion reactions with radioactive beams and could provide important information on large systems of astrophysical interest.

5.2 Neutron stars: structure and equation of state

A large amount of information on neutron stars should be available in the next few years from the new generation of X– and γ–ray satellites. In view of this, neutron stars are the subject of many theoretical studies, aimed to predict their structure on the basis of the properties of dense matter. The equation of state (EOS) of neutron stars covers a wide density range, from ~ 10 g/cm^3 in the surface to several times nuclear matter saturation density ($\rho \equiv \rho_0 \sim 2.8 \times 10^{14}$g/cm^3) in the center of the star.

The core (interior part) of a neutron star is believed to consist of asymmetric nuclear matter with a consistent fraction of leptons. At ultra–high densities, matter might undergo a transition giving rise to other exotic hadronic components, like hyperons, a K^- condensate or a deconfined phase of quark matter. This occurrence, in turn, could critically influence the evolution of neutron stars and could eventually lead to the formation of black holes.[31]

Baldo *et al.* have derived the static properties of non–rotating neutron stars in a conventional framework, using the microscopic EOS for asymmetric nuclear matter, derived from the Brueckner–Bethe–Goldstone many–body theory.[32] They use the Argonne V_{14} and the Paris two–body interactions, implemented by the Urbana model for the three–body force. The latter are incorporated into the Brueckner scheme by reducing them to affective two–body, density dependent forces. The parameters are adjusted to reproduce the empirical nuclear matter saturation point.

The calculated EOS allows to compute masses and radii as a function of the central density n_0. Assuming that a neutron star is a spherically symmetric distribution of mass in hydrostatic equilibrium, and neglecting the effects of rotations and magnetic field, the equilibrium configurations are obtained by solving the Tolman– Oppenheimer–Volkoff (TOV) equations for the total pressure and the enclosed mass:

$$\frac{dP(r)}{dr} = -\frac{Gm(r)\rho(r)}{r^2}\frac{\left(1 + \dfrac{P(r)}{c^2\rho(r)}\right)\left(1 + \dfrac{4\pi r^3 P(r)}{c^2 m(r)}\right)}{\left(1 - \dfrac{2Gm(r)}{rc^2}\right)} \tag{5.33}$$

$$\frac{dm(r)}{dr} = 4\pi r^2 \rho(r), \tag{5.34}$$

where G is the gravitational constant. The maximum mass configuration obtained in ref.[32] range from 1.8 to 2.13 solar masses, while the corresponding radii vary from 8 to 10.6 Km. These values are consistent with the present observations.

A challenging suggestion is found in a work of Bombaci[33], concerning the semiempirical mass–radius relation extracted for the X–ray burst source 4U 1820–30: the latter cannot be reproduced by neutron star models based on conventional EOS. It is thus suggested that the onset of a phase transition to a K^- condensate could explain, with a suitable choice of the parameters, the observed mass–radius relation.

5.3 Neutron stars: the effects of superfluidity

As already mentioned in the above subsections, it is believed that the inner crust of a neutron star, at a density of about 3×10^{11} g/cm^3 (corresponding to about $10^{-3}\rho_0$), is a superfluid and inhomogeneous system, consisting of a lattice of nuclei immersed in a sea of neutrons and an approximately uniform sea of electrons. Such a configuration persists up to roughly $\rho_0/2$. At low temperatures, this system is superfluid with a positive Fermi energy ϵ_F: the estimate of the pairing gap in this inhomogeneous medium has been carried out by Barranco *et al.*[34]. They solve the Hartree–Fock–Bogoliubov (HFB) equations in a Wigner–Seitz cell, with a Woods–Saxon potential; the gap is calculated self–consistently without altering the single particle levels. Use is made of the Argonne two–body interaction.

The HFB method is suitable to describe the halo–nuclei and/or neutron–rich nuclei. Surface collective modes (phonons) mediate the induced interaction producing Cooper pairs and a bosonic condensate.

In a second work[35] the quantum calculation is compared to the LDA. Here the two–body interaction is assumed to be a Gogny force and is included in the HFB equations via the pairing field.

It is found that the LDA leads to a spatial variation of the gap near the surface of a nucleus, which is stronger than the one obtained in the HFB calculation. This is caused by the neglect of the proximity effects and the delocalized character of the single–particle wave functions close to the fermi energy.

From the energy of the system,

$$< E > = \sum_q n_q E_q, \tag{5.35}$$

where $n_q = (1 + e^{E_q/T})^{-1}$ is the occupation number (at the temperature T) for the quasi–particle state q, one can obtain the *specific heat* of the system:

$$C_v = \frac{1}{V} \frac{\partial < E >}{\partial T}. \tag{5.36}$$

This quantity turns out to be very sensitive to the pairing gap, and hence to the presence of the inhomogeneity induced by the presence of the nuclei in the crust. The overestimate of the gap, as obtained in LDA, leads to a specific heat of the system which is too large at low temperatures, as compared with the quantal result. Incidentally, a reliable estimate of the pairing gap is also important for the determination of the cooling time of the neutron star.

In concluding this argument, it is worth mentioning that pairing correlations have been studied within a relativistic mean field approach based on a field theory of nucleons coupled to neutral (σ and ω) and charged (ρ) mesons. The HF and pairing fields are calculated in a self–consistent way[36]. The energy gap is the result of strong cancellations between the scalar and vector components of the pairing field. It is found that the pair amplitude vanishes beyond a certain value of momentum of the paired nucleons; the estimated gap is in agreement with non–relativistic calculations of this quantity.

5.4   Neutron stars: massive quark matter

While in the previous subsection the attention was focussed on the surface region of a neutron star, where the low density advocates nucleonic degrees of freedom, its high central density, up to $5 \div 10 \, \rho_0$, seems to imply the existence of a core of massive quark matter. The latter can be described in a variety of different models, among which we shall consider here the so–called Color Dielectric Model (CDM), which has been successfully employed in connection with the single nucleon properties (structure functions, e.m. form factors) as well as for the nucleon–nucleon interaction.

The CDM entails confinement of the quarks in ordinary hadronic matter but also allows to describe, in mean field approximation, a phase transition to deconfined quark matter[37, 38, 39]. The model is defined by the following Lagrangian:

$$
\begin{aligned}
\mathcal{L} \; =\; & i\bar{\psi}\gamma^{\mu}\partial_{\mu}\psi + \sum_{f=u,d} \frac{g_f}{f_\pi \chi} \bar{\psi}_f \left(\sigma + i\gamma_5 \tau \cdot \pi \right) \psi_f \\
& + \frac{g_s}{\chi} \bar{\psi}_s \psi_s + \frac{1}{2} \left(\partial_\mu \chi \right)^2 - \frac{1}{2} \mathcal{M}^2 \chi^2 \\
& + \frac{1}{2} \left(\partial_\mu \sigma \right)^2 + \frac{1}{2} \left(\partial_\mu \pi \right)^2 - U(\sigma, \pi)
\end{aligned}
\tag{5.37}
$$

where χ is the color dielectric field and $U(\sigma, \pi)$ the "mexican hat" potential of the chiral sigma–model. This Lagrangian describes a system of interacting u, d and s quarks, pions, sigmas and a scalar–isoscalar chiral singlet field χ. The latter is related to the fluctuations of the gluon condensate around its vacuum expectation value. The coupling constants are given by $g_{u,d} = g(f_\pi \pm \xi_3)$ and $g_s = (2f_K - f_\pi)$, where $f_\pi = 93$ MeV and $f_K = 113$ MeV are the pion and kaon decay constants, respectively, while $\xi_3 = f_{K^\pm} - f_{K^0} = -0.75$ MeV. Hence the model contains only two free parameters, g and $\mathcal{M}$, which are fixed to the values $g = 0.023$ GeV, $\mathcal{M} = 1.7$ GeV. Confinement is obtained via the effective quark masses, which diverge outside the nucleon.

The CDM is employed to describe the deconfined quark matter phase in the neutron star, while the relativistic field theoretical model of Walecka is used for the hadronic phase. Applying Gibbs criteria to this composite system, Drago *et al.*[38] find that the pure hadronic phase ends at 0.11 fm^{-3} while the mixed (quark and hadronic) phase extends up to 0.31 fm^{-3}.

According to this calculation, neutron stars with masses in the range $1.3 < M/M_\odot < 1.54$ and radii of about 9 Km are found. A neutron star with total mass of $1.4 \, M_\odot$ will consist of a crust of pure hadronic matter, a ~ 1 Km thick region of mixed phase and a core of pure quark matter.

In a recent work[39] the EOS of quark matter based on the CDM has been discussed, taking into account the effects associated with finite temperatures. Both the evolution of neutron stars and the onset of supernovae explosion crucially depend upon the EOS of matter at very high densities and temperatures. At finite T the EOS considered here shows a decrease of the pressure and of

the adiabatic index, leading to a deconfinement transition for densities slightly larger than the one corresponding to nuclear matter saturation. The presence of a mixed phase region softens the EOS and could lead to a direct supernova explosion. At larger densities the EOS is stiff enough to support a neutron star compatible with observations.

6   Quark matter

Quantum Chromodynamics (QCD), the non–abelian theory of coloured quarks and gluons, is currently accepted as the theory of strong interactions, and its predictions have been tested in a variety of elementary particle reactions at large momentum transfers. Its behaviour in the high energy (or short distance) limit approaches the one of a non–interacting free field theory (*asymptotic freedom*), while at low energies (or large length scales) QCD is a non–perturbative field theory, quarks and gluons being permanently confined inside hadrons.

At very high nuclear densities and/or temperatures it is believed that hadronic matter undergoes a phase transition to a deconfined phase of quarks and gluons, the so–called Quark Gluon Plasma (QGP). In this new phase hadrons dissolve, strong interactions become very weak and an ideal colour–conducting plasma of quarks and gluons is formed. In the QGP the long–range colour force is Debye–screened due to collective effects and the quarks can only interact via a short–range effective potential.

During the last decade the attention of nuclear and particle physics has been attracted by the possibility of producing this new state of matter in the laboratory, by means of ultra–relativistic heavy ion collisions. A large number of experiments have been carried out at the AGS (Brookhaven) and at the SPS (CERN). Both laboratories have planned considerable "upgrading" of the existing facilities, the so–called RHIC (Relativistic Heavy Ion Collider), which is going into operation in 1999 and the LHC (Large Hadron Collider), whose program will be partly dedicated to high energy particle physics and partly to heavy ion collisions. The most recent measurements refer to S+U reactions at 200 GeV/A and Pb+Pb at 158 GeV/A, reaching an (estimated) energy density of $2 \div 5$ GeV/fm^3.

Many aspects of the transition from hadrons to deconfined quark matter, among which the order of the phase transition and the nature of experimentally observable signatures, are still under debate. Recently the NA50 experiment at CERN[40] has shown an anomalous suppression of the J/Ψ survival probability measured in Pb on Pb collisions[41], which might be ascribed to the formation of QGP at some stage of the collision. Other interesting signals could be revealed by the dilepton spectra, which are sensitive to the masses of vector mesons: the latter can be significantly altered by the presence of the QGP, an argument which is still widely discussed.

6.1   Quark deconfinement

At high densities and temperatures, the interaction between quarks and gluons dresses their propagation, so that gluons develop an effective mass, which in turn produces screening of the long–range colour–electric forces. For example, the free gluon propagator $D_0(\omega, k) \sim (\omega^2 - k^2)^{-1}$ is modified by summing an infinite chain of one–loop insertions. One obtains[42] the following longitudinal gluon propagator

$$D_L(\omega, k) = \frac{1}{k^2 \varepsilon_L(\omega, k)} \tag{6.38}$$

D_L being a scalar function of the variables $\omega = k^0$ and $k = |\mathbf{k}|$ and ε_L the so–called colour dielectric function. From explicit calculations, one can show that the static ($\omega = 0$) longitudinal colour fields are screened, being

$$D_L(0, k) = \frac{1}{k^2 \varepsilon_L(0, k)} = \frac{1}{k^2 + g^2 T^2} \equiv \frac{1}{k^2 + \lambda_D^{-2}} \tag{6.39}$$

which defines the Debye length $\lambda_D = (gT)^{-1}$.

The above mentioned features of the gluon propagator entail several important consequences, among which we focus here on the fact that the potential between two static colour charges (e.g. two heavy quarks) is *screened* in the quark–gluon plasma phase. Indeed the Fourier transform of $D_L(0, k)$, eq.(6.39), yields the potential

$$V_{Q\bar{Q}}(r) \simeq \frac{1}{r} e^{-r/\lambda_D} \tag{6.40}$$

with screening length $\lambda_D \simeq 0.4$ fm at $T = 250$ MeV. This screening of the long range colour forces is believed to be at the origin of quark deconfinement in the high temperature phase. It also leads to the disappearence of the bound states of a charmed quark pairs ($c\bar{c}$) in the QGP[43].

Fig. 10 illustrates the deconfinement effect of a thermodynamical enviroment of interacting light quarks and gluons on the interquark potential employed in ref.[44] to investigate the deconfinement conditions for heavy quarkonia.:

$$V(r, T) = \frac{\sigma}{\mu(T)} \left(1 - e^{\mu(T)r} \right) - \frac{\alpha}{r} e^{-\mu(T)r} \tag{6.41}$$

where $\mu(T) = 1/\lambda_D(T)$. The potential (6.41) reduces to the Cornell potential in the zero temperature limit (we remind that $\lambda_D \to \infty$ for $T \to 0$); in addition to the one gluon exchange contribution ($1/r$) this potential also contains a phenomenological linear binding term, as suggested by lattice QCD calculations for the interaction between static (heavy) colour charges.

It would be important to find some "QCD inspired" model, suitable to describe both the confined (hadronic) and the deconfined (plasma) phases of a system of *many* quarks. This is obviously not trivial to achieve, due to the non–perturbative nature of the quark–quark interaction in the confined phase and also to the unavoidable approximations required to describe a many–body system, even when the interactions are known.
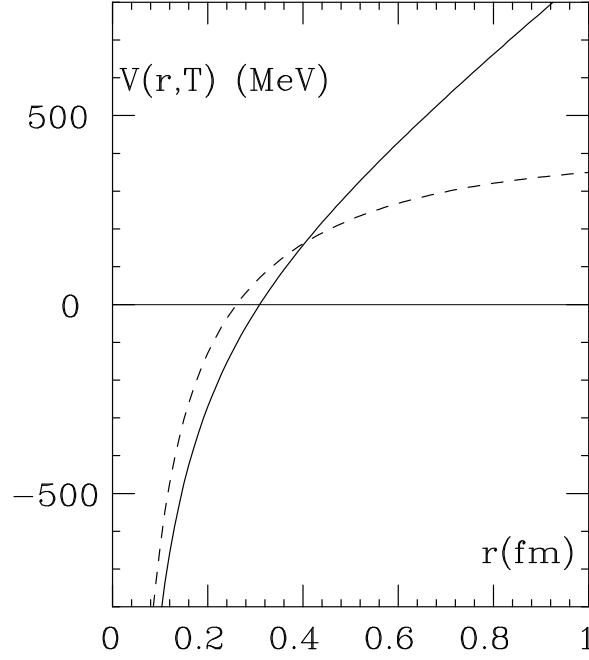
Fig. 10. The quark–quark potential, eq.(6.41) at $T = 250°$ (dashed line) and $T = 0$ (continuous line).

In a recent work Alberico *et al.*[45] have developed a three–dimensional model for quark matter with a *density dependent* quark–quark (confining) potential, which allows to describe a sort of deconfinement transition as the system evolves from a low density assembly of bound structures to a high density free Fermi gas of quarks. Different confining potentials are considered, some of which successfully utilized in hadron spectroscopy, like the Cornell one.

We find that a proper treatment of the many–body correlations induced by the medium is essential to disentangle the different nature of the two (hadronic and deconfined) phases of the system. For this purpose the ground state energy per particle and the pair correlation function are investigated. The latter can be obtained from the expectation value of the two–body density operator:

$$g(r) = \frac{N(N-1)}{\rho^2} < \Psi|\rho_2(|\mathbf{r}_1 - \mathbf{r}_2|)|\Psi >, \qquad (6.42)$$

where $|\Psi >$ is the exact (normalized) ground state of the system. For a system of strongly correlated pairs $g(r)$ will show up a well localized peak at small values of r, while the Fermi gas pair correlation function has a fairly constant behaviour,

with the exception of small r values, where the Pauli principle prevents particles to be close to each other.

As an example, Fig. 11 shows the pair correlation function derived from the Bethe–Goldstone wave functions of the screened Cornell potential:

$$V_{Cornell}(r,\rho) = \left(-\frac{a}{r} + br + K\right) e^{-c\rho r} \tag{6.43}$$

where a, b, c and K are constants, while ρ is the density of the system. The free Fermi gas two–body correlation function is recovered for $\rho \simeq 0.6$ fm^{-3}, in agreement with the value of the "transition density" which can be obtained from the corresponding equation of state.
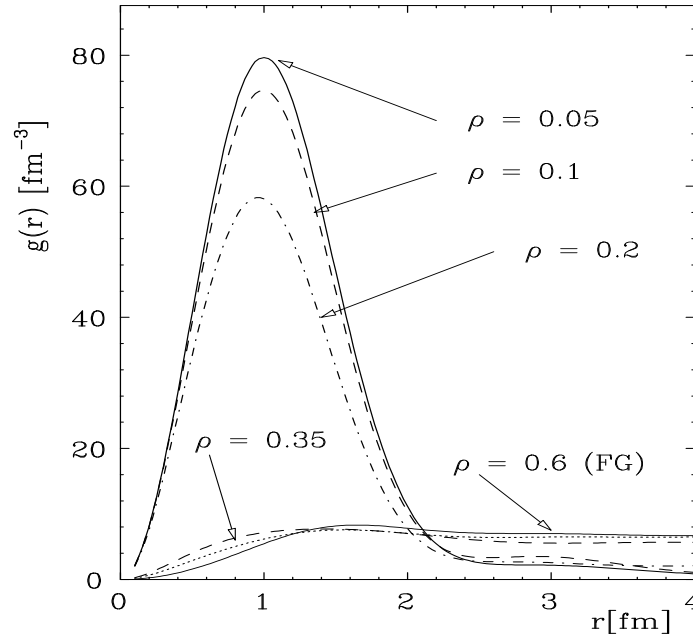

Fig. 11. The pair correlation function $g(r)$ obtained with the potential (6.43) is displayed as a function of the relative interquark distance at various densities: $\rho = 0.05$ fm^{-3} (thick solid line), $\rho = 0.1$ fm^{-3} (dashed line), $\rho = 0.2$ fm^{-3} (dot–dashed line), $\rho = 0.35$ fm^{-3} (dashed line) and $\rho = 0.6$ fm^{-3} (dotted line). For the last density value the Fermi gas correlation function is also shown (thin solid line).

6.2   Finite size effects in the QGP

Before concluding this Section it is worth mentioning that one of the major difficulties in the analysis of the relativistic heavy ion collisions stems from the

numerous uncertainties in the thermostatistical evolution of the system. Among the various steps, the hadronization process is crucial in determining the final states measured in the detectors.

Brink *et al.*[46] have studied the hadronization of a plasma, in order to establish whether the final particles are evaporated from droplets of hadronic matter inside the plasma or rather from the whole volume of the plasma itself. The two situations can be distinguished on the basis of the entropy density of the system.

Let us assume that at equilibrium (close to the critical temperature $T \sim T_c$) the volume of the plasma (V_{tot}) is filled by N droplets of QGP (each occupying a volume V_{glob}) and a gas of relativistic pions. For a fixed total volume and energy density, the calculated entropy density of the systems turns out to be larger when the plasma fills a big, unique glob rather than several globs of smaller radius. This is partially illustrated in Fig. 12. Finite size corrections are taken into account in the density of levels which enters into the calculation of the entropy. Fluctuations with respect to the number of globs are small, hence there is no tendency for a large glob to break spontaneously into smaller ones.
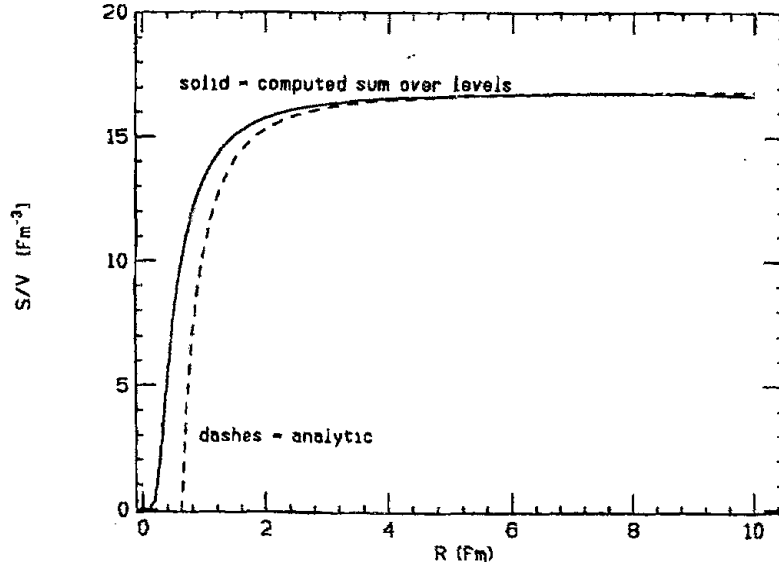

Fig. 12. Entropy density for a gas of quarks and gluons as a function of the glob radius R. The temperature is fixed to be $T = 200$ MeV.

This argument concludes the tour which was foreseen in the introduction, showing how the various many–body techniques can be applied to strongly interacting systems, either of nucleons or of quarks, in an attempt to provide a

unified microscopic description of the intriguing, complex structure of nuclear systems.

Acknowledgments

I would like to thank Dr. A. de Pace and Prof. A. Molinari for enlightening discussions and to acknowledge their valuable help.

References

1. J.E. Amaro, M.B. Barbaro, J.A. Caballero, T.W. Donnelly and A. Molinari, Nucl. Phys. **A643**, 349 (1998)
2. R. Cenni, T.W. Donnelly and A. Molinari, Phys. Rev. **C56**, 276 (1997)
3. W.M. Alberico, G. Chanfray, J. Delorme, M. Ericson and A. Molinari, Nucl. Phys. **A634**, 233 (1998)
4. See the contribution of C. Ciofi degli Atti to these Proceedings
5. More details can be found in the contribution of M.B. Barbaro to these Proceedings
6. W.M. Alberico, M.B. Barbaro, S.M. Bilenky, J.A. Caballero, C. Giunti, C. Maieron, E. Moya de Guerra and J.M. Udias, Nucl. Phys. **A623**, 471 (1997)
7. W.M. Alberico, M.B. Barbaro, S.M. Bilenky, J.A. Caballero, C. Giunti, C. Maieron, E. Moya de Guerra and J.M. Udias, Phys. Lett. **B 438**, 9 (1998)
8. W.M. Alberico, M.B. Barbaro, S.M. Bilenky, J.A. Caballero, C. Giunti, C. Maieron, E. Moya de Guerra and J.M. Udias, e-Print hep-ph/9812388 (Dec. 1998)
9. A. Fabrocini, Phys. Rev. **C55**, 338 (1997)
10. R.B. Wiringa, V. Fiks and A. Fabrocini, Phys. Rev. **C38**, 1010 (1988)
11. R. Schiavilla, V.R. Pandharipande and D.O. Riska, Phys. Rev. **C40**, 2294 (1989)
12. Z. Meziani *et al.*, Phys. Rev. Lett. **52**, 2130 (1984)
13. T.C. Yates *et al.*, Phys. Lett. **B312**, 382 (1993)
14. J. Jourdan, Nucl. Phys. **A603**, 117 (1996)
15. J.E. Amaro, A.M. Lallena, G. Cò and A. Fabrocini, Phys. Rev. **C57**, 3473 (1998)
16. R. Cenni, F. Conte and P. Saracco, Nucl. Phys. **A623**, 391 (1997)
17. T.S. Wahlhout, R. Cenni, A. Fabrocini and S. Fantoni, Phys. Rev. **C54**, 1622 (1996)
18. A. De Pace, Nucl. Phys. **A** (1998)
19. M.B. Barbaro, A. De Pace, T.W. Donnelly and A. Molinari, Nucl. Phys. **A598**, 503 (1996)
20. M.B. Barbaro, R. Cenni, A. De Pace, T.W. Donnelly and A. Molinari, Nucl. Phys. **A643**, 137 (1998)
21. B.D. Serot and J.D. Walecka, Int. J. Mod. Phys. **E6**, 515 (1997)
22. P. Amore, R. Cenni, T.W. Donnelly and A. Molinari, Nucl. Phys. **A615**, 353 (1997)
23. A. De Pace, C. Garcia–Recio and E. Oset, Phys. Rev. **C55**, 1394 (1997)
24. J.A. Oller, E. Oset, A. De Pace and P. Fernandez de Cordoba, Phys. Rev. **C57**, 1404 (1998)
25. A. De Pace, in *Proceed. of the Int. Conf. on Hypernuclear and Strange Particle Physics*, Brookhaven Nat. Lab., Oct. 1997
26. C.M. Kormanyos *et al.*, Phys. Rev. **C51**, 669 (1995)
27. G. Garbarino, W.M. Alberico, A. De Pace and A. Ramos, in preparation

28. G. Cò and A. Fabrocini, work in progress
29. V. Baran, M. Colonna, M. Di Toro, A.B. Larionov, Nucl. Phys. **A632**, 287 (1998)
30. M. Di Toro, M. Colonna, V. Baran, A.B. Larionov, *Int. Conf. on Giant Resonances*, Varenna 1998, Nucl. Phys. A; see also the contribution of M. Di Toro *et al.* in these Proceedings
31. Madappa Proakash, I. Bombaci, Manju Prakash, P.J. Ellis, J.M. Lattimer and R, Knorren, Phys. Reports **280**, 1 (1997)
32. M. Baldo, I. Bombaci and G.F. Burgio, Astron. Astrophys. **328**, 274 (1997)
33. I. Bombaci, Phys. Rev. **C55**, 1587 (1997)
34. F. Barranco, H. Esbensen, E. Vigezzi and R.A. Broglia, Phys. Lett. **B390**, 13 (1997)
35. F. Barranco, R.A. Broglia, H. Esbensen and E. Vigezzi, e-print nucl-th/9806056
36. F. Matera, G. Fabbri and A. Dellafiore, Phys. Rev. **C57** (1997)
37. A. Drago, M. Hjorth-Jensen and U. Tambini, Prog. Part. Nucl. Phys. **36**, 407 (1996)
38. A. Drago, U. Tambini and M. Hjorth–Jensen, Phys. Lett. **B380**, 13 (1996)
39. A. Drago and U. Tambini, preprint, March 1998
40. M. Gonin, NA50 Collaboration, Nucl. Phys. **A610**, 404c
41. D. Kharzeev, C. Lourenco, M. Nardi and H. Satz, Z. Physik **C 74**, 307 (1997)
42. J. Kapusta, Nucl. Phys. **B148**, 461 (1979)
43. T. Matsui and H. Satz, Phys. Lett. **B 178**, 416 (1986)
44. F. Karsch, M.T. Mehr and H. Satz, Z. Physik **C 37**, 617 (1988)
45. W.M. Alberico, P. Czerski and M. Nardi, Eur. Journ. Phys. **A** (1999), in press
46. D.M. Brink and Lo Monaco, J. Phys. **G 24**, 867 (1988)